Chapter 2

Cattanneo-Christov Heat Flux Model Study for Water-Based CNT Suspended Nanofluid Past a Stretching Surface

Noreen Sher Akbar, C. M. Khalique and
Zafar Hayat Khan

Additional information is available at the end of the chapter

http://dx.doi.org/10.5772/65628

Abstract

This chapter discusses the magnetic field effects on the flow of Cattanneo-Christov heat flux model for water-based CNT suspended nanofluid over a stretching sheet. According to the authors, knowledge idea of Cattanneo-Christov heat flux model for water-based CNT suspended nanofluid is not explored so far for stretching sheet. The flow equations are modeled for the first time in the literature transformed into ordinary differential equations using similarity transformations. The numerical solutions are computed using shooting technique and compared with the literature for the special case of pure fluid flow and found to be in good agreement. Graphical results are presented to illustrate the effects of various fluid flow parameters on velocity, heat transfer, Nusselt number, Sherwood number, and skin friction coefficient for different types of nanoparticles.

Keywords: boundary layer flow, nanofluid, stretching sheet, Cattanneo-Christov heat flux model, numerical solution

1. Introduction

From recent few decades, heat transfer enhancement of the nanofluid has turned out to be a topic of main interest for the researchers and scientists. The word "nanofluid" was derived by Choi [1]. He defines a liquid suspension comprising ultrafine particles whose diameter is less than 50 nm. Xuan and Roetzel [2] investigated the mechanism of heat transfer enhancement of the nanofluid. According to them, the nanofluid is a solid-liquid mixture in which metallic or

INTECH
open science | open minds

© 2017 The Author(s). Licensee InTech. This chapter is distributed under the terms of the Creative Commons Attribution License (http://creativecommons.org/licenses/by/3.0), which permits unrestricted use, distribution, and reproduction in any medium, provided the original work is properly cited. CC BY

nonmetallic nanoparticles are suspended. The suspended ultrafine particles change transport properties and heat transfer performance of the nanofluid, which exhibits a great potential in enhancing heat transfer. They found that the reduced Nusselt number is a decreasing function of each nanofluid parameters. Khanafer et al. [3] discussed buoyancy-driven heat transfer enhancement in a two-dimensional enclosure utilizing nanofluids. The natural convective boundary-layer flow of a nanofluid over a vertical plate is studied analytically by Kuznetsov and Nield [4]. Boundary layer laminar nanofluid flow over the stretching flat surface has been investigated numerically by Khan and Pop [5]. They show that the reduced Nusselt number is a decreasing function of each dimensionless number, while the reduced Sherwood number is an increasing function of higher Prandtl number. Ebaid and his co-authors [6–10] present boundary-layer flow of a nanofluid past a stretching sheet with different flow geometries and with different conditions. Wang [11] discussed free convection on a vertical stretching surface. Scaling group transformation for MHD(Magneto hydrodynamic) boundary-layer flow of a nanofluid past a vertical stretching surface in the presence of suction/injection was discussed by Kandasamy et al. [12].

Fourier [13] was the first who discussed the heat transfer phenomenon in 1822. The equation presented by him was parabolic in nature and has draw back that in initial disturbance is felt instantly throughout the whole medium. Cattaneo [14] modifies the "Fourier law of heat conduction in which he added the thermal relaxation term. The addition of thermal relaxation time causes heat transportation in the form of thermal waves with finite speed." Christov [15] in this contest discussed Oldroyd upper-convected derivative as an alternative of time plagiaristic to complete the material-in variant formulation. This model is known as Cattaneo-Christov heat flux model. Tibullo et al. [16] described the uniqueness of Cattaneo-Christov heat flux model for incompressible fluids. Mustafa [17] presented the Cattaneo-Christov heat flux model for Maxwell fluid over a stretching sheet. According to him, velocity is inversely proportional to the viscoelastic fluid parameter. Further, fluid temperature has inverse relationship with the relaxation time for heat flux and with the Prandtl number. Very recently, Salahuddin et al. [18] discussed MHD flow of Cattanneo-Christov heat flux model for Williamson fluid over a stretching sheet with variable thickness. They solved nonlinear problem numerically by using implicit finite difference scheme known as Keller box method. They observed that large values of wall thickness parameter and Weissenberg number are suitable for reduction in velocity profile. For further details, see Refs. [11, 12, 19–32].

The aim of this chapter is to discuss the magnetic field effects on the flow of Cattanneo-Christov heat flux model for water-based CNT suspended nanofluid over a stretching sheet. Because according to the authors, knowledge idea of Cattanneo-Christov heat flux model for water-based CNT suspended nanofluid is not explored so far for stretching sheet. The flow equations are modeled for the first time in the literature transformed into ordinary differential equations using similarity transformations. The numerical solutions are computed using shooting technique and compared with the literature for the special case of pure fluid flow and found to be in good agreement. Graphical results are presented to illustrate the effects of various fluid flow parameters on velocity, heat transfer, Nusselt number, Sherwood number, and skin friction coefficient for different types of nanoparticles.

http://dx.doi.org/10.5772/65628

2. Formatting mathematical model

We discuss the two-dimensional nanofluid flow over a stretching sheet with water as based fluids surrounding single- and multi-wall CNTs. The flow is supposed to be laminar, steady, and incompressible. The base fluid and the CNTs are usual to be in updraft stability. Sheet is whispered to be stretched with the dissimilar velocity U_w, V_w along the x-axis and y-axis, correspondingly. We have taken the invariable ambient temperature T_∞. Supplementary new heat model named as Cattanneo-Christov heat flux model is considered to analyze heat transfer phenomena. The x-axis is taken along the sheet, and y-axis is chosen normal to it. Magnetic field of strength B_0 is applied normal to the sheet (as shown in **Figure 1**).

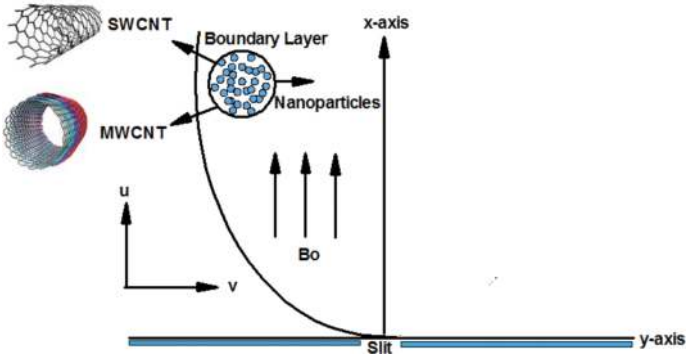

Figure 1. Physical model for the magnetohydrodynamic nanofluid stretching sheet problem.

With the above analysis, the boundary layer equations for the proposed model, i.e., continuity, momentum, and energy equations, can be written as follows:

$$\frac{\partial u}{\partial x}+\frac{\partial v}{\partial y}=0, \tag{1}$$

$$\left(u\frac{\partial u}{\partial x}+v\frac{\partial u}{\partial y}\right)=\nu_{nf}\left(\frac{\partial^2 u}{\partial y^2}\right)-\frac{\sigma_{nf}B_o^2}{\rho_{nf}}u, \tag{2}$$

$$\rho_{nf}\left(c_p\right)_{nf}\bar{v}.\nabla T=-\nabla.q, \tag{3}$$

where u and v are the velocity components along x and y directions, respectively, T is the temperature of the fluid, B_0 is the magnitude of magnetic field, and q is the heat flux. Equation (3) is the Cattaneo-Christov flux model and has the following form:

$$q+\lambda_2\left(\frac{\partial q}{\partial t}+V.\nabla.q-q.\nabla V+\left(\nabla.V\right)q\right)=-K_{nf}\nabla T, \tag{4}$$

where λ_2 is the thermal relaxation time. Eliminating q from Eqs. (3) and (4) gives as follows:

$$\begin{aligned}&\left(u\frac{\partial T}{\partial x}+v\frac{\partial T}{\partial y}\right)+\lambda_2\left(\begin{array}{l}u\frac{\partial u}{\partial x}\frac{\partial T}{\partial x}+v\frac{\partial v}{\partial y}\frac{\partial T}{\partial y}+u\frac{\partial v}{\partial x}\frac{\partial T}{\partial y}+v\frac{\partial u}{\partial y}\frac{\partial T}{\partial x}\\+2uv\frac{\partial^2 T}{\partial x\partial y}+u^2\frac{\partial^2 T}{\partial x^2}+v^2\frac{\partial^2 T}{\partial y^2}\end{array}\right)\\&=\frac{K_{nf}}{\rho_{nf}\left(c_p\right)_{nf}}\frac{\partial^2 T}{\partial y^2},\end{aligned} \tag{5}$$

Further, ρ_{nf} is the effective density, μ_{nf} is the effective dynamic viscosity, $(\rho c_p)_{nf}$ is the heat capacitance, α_{nf} is the effective thermal diffusibility, and k_{nf} is the effective thermal conductivity of the nanofluid, which are defined as follows:

$$\begin{aligned}&\rho_{nf}=\left(1-\phi\right)\rho_f+\phi\,\rho_{CNT},\mu_{nf}=\frac{\mu_f}{\left(1-\phi\right)^{2.5}},\alpha_{nf}=\frac{k_{nf}}{\left(\rho_{cp}\right)_{nf}},\\&\left(\rho_{cp}\right)_{nf}=\left(1-\phi\right)\left(\rho_{cp}\right)_f+\phi\left(\rho_{cp}\right)_{CNT},\\&k_{nf}=k_f\left(\frac{\left(1-\phi\right)+\frac{2\varphi k_{CNT}}{k_{CNT}-k_f}\log\left(\frac{k_{CNT}+k_f}{2k_f}\right)}{\left(1-\phi\right)+\frac{2\varphi k_f}{k_{CNT}-k_f}\log\left(\frac{k_{CNT}+k_f}{2k_f}\right)}\right),\end{aligned} \tag{6}$$

where μ_f is the viscosity of base fluid, ϕ is the nanoparticles fraction, $(\rho C_p)_f$ is the effective heat capacity of a fluid, $(\rho C_p)_{CNT}$ is the effective heat capacity of a carbon nanotubes, k_f and k_{CNT} are the thermal conductivities of the base fluid and carbon nanotubes, respectively, ρ_f and ρ_{CNT} are the thermal conductivities of the base fluid and carbon nanotubes, respectively.

Corresponding boundary conditions are as follows:

$$u=ax+N\nu_f\frac{\partial u}{\partial y},v=0,T=T_w,\ \text{at}\ y=0, \tag{7a}$$

$$u\to 0,v\to 0,T\to T_\infty,\ \text{as}\ y\to\infty.zd \tag{7b}$$

where T, T_w and N are the ambient, wall fluid temperature, and slip parameter, respectively.

Introducing the following similarity transformations, we have

http://dx.doi.org/10.5772/65628

$$\eta = \sqrt{\frac{a}{\nu_f}}y,\ u = axf'(\eta),\ v = -\sqrt{a\nu_f}f(\eta), \theta = \frac{T - T_\infty}{T_f - T_\infty} \tag{8}$$

Making use of Eqs. (6, 8) in Eqs. (1–5), we have

$$f''' + (1-\phi)^{2.5}\left[\left(1-\phi+\phi\frac{\rho_{CNT}}{\rho_f}\right)\left\{ff'' - f'^2\right\} - M^2 f'\right] = 0, \tag{9}$$

$$\left(\frac{k_{nf}}{k_f}\right)\theta'' + \Pr\left(1-\phi+\phi\frac{(\rho c_p)_{CNT}}{(\rho c_p)_f}\right)\left[(f\theta') - \gamma\left(ff'\theta' + f^2\theta''\right)\right] = 0, \tag{10}$$

$$f(0) = 0,\ f'(0) = 1,\ f'(\infty) = 0, \theta(0) = 1,\ \theta(\infty) = 0, \tag{11}$$

where $\Pr = \dfrac{(\mu c_p)_f}{k_f}$ is the Prandtl number, $\gamma = a\lambda_2$ is the non-dimensional thermal relaxation time, and $\beta = N\sqrt{a\nu_f}$ is the slip parameter.

The quantity of practical interest, in this study, is the skin friction coefficient c_f and Nusselt number Nu_x, which is defined as follows:

$$c_f = \frac{\mu_{nf}}{\rho_f U_w^{\ 2}}\left(\frac{\partial u}{\partial y}\right)_{y=0}, Nu_x = \frac{-xK_{nf}}{k_f(T_f - T_\infty)}\left(\frac{\partial T}{\partial y}\right)_{y=0} \tag{12}$$

where q_w is the heat flux and K_{nf} is the effective thermal conductivity. Using variables (8), we obtain:

$$\mathrm{Re}_x^{1/2} c_f = \frac{f''(0)}{(1-\phi)^{2.5}},\quad \mathrm{Re}_x^{-1/2} Nu_x = -\frac{k_{nf}}{k_f}\theta'(0). \tag{13}$$

3. Numerical scheme

The nonlinear ordinary differential equations (9)–(10) subject to the boundary conditions (11) have been solved numerically using an efficient Runge-Kutta fourth-order method along with shooting technique. The asymptotic boundary conditions given by Eq. (11) were replaced by using a value of 15 for the similarity variable $\eta_{\max}$. The choice of $\eta_{\max}$ = 15 and the step size

$\Delta\eta = 0.001$ ensured that all numerical solutions approached the asymptotic values correctly. For validating of the proposed scheme, a comparison for the Nusselt number with the literature [4, 8, 9] has been shown in **Table 2** for both active and passive control of ϕ in the special case when. Therefore, we are confident that the applied numerical scheme is very accurate.

4. Results and discussion

In this section, the graphical explanation of the numerical results for velocity, temperature, skin friction coefficients, Nusselt number, and stream lines is expressed with respect to certain changes in the physical parameters through illustrations (**Figures 2–7**). A comparative study for pure water, SWCNT and MWCNT, is also depicted through **Tables 1–5**.

(**Figure 2a** and **b**) represents the changes in the fluid velocity profiles with respect to different values of solid nanoparticle volume fraction. **Figure 2(a)** shows the variation in solid volume fraction of nanoparticles with respect to Hartmann number M. As Hartmann number is the ratio of electromagnetic forces to the viscous forces. It is observed that when Hartmann number increases, electromagnetic forces will be dominant to the viscous forces that give declines in the velocity field (see **Figure 2(a)**). **Figure 2(b)** shows the variation in solid nanoparticle volume fraction with slip parameter β on velocity profile. It is analyzed that with an increase in slip parameter, velocity profile decreases. Further with an increase in solid nanoparticle volume fraction, velocity profile increases, and boundary layer thickness also increases with the increase in Hartmann number M, slip parameter, and solid nanoparticle volume fraction.

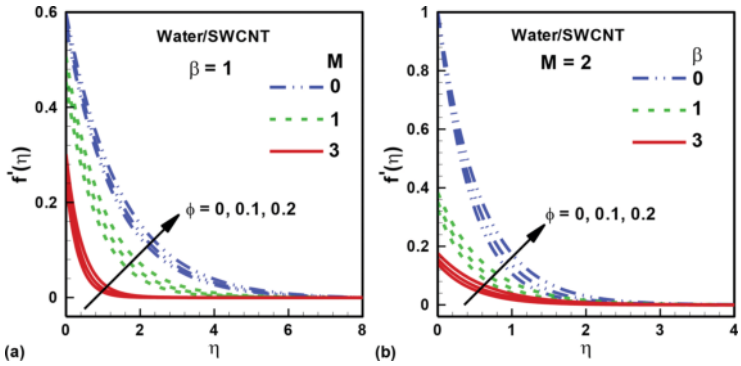

Figure 2. Velocity profile for different values of solid nanoparticle volume fraction. (a) Shows the variation with Hartmann number M. (b) Shows the variation with slip parameter β.

Temperature profile for different values of solid nanoparticle volume fraction with the variation in thermal relaxation time γ, Hartmann number M, and slip parameter β is presented in **Figure 3**(**a–c**). Temperature profile decreases with the rise in thermal relaxation time, but thermal boundary layer increases with an increase in thermal relaxation time (see **Figure 3(a)**).

http://dx.doi.org/10.5772/65628

Figure 3(b) depicts that with an increase in electromagnetic forces as compared to the viscous forces, temperature profile and thermal boundary layer increase rapidly. Temperature profile and thermal boundary layer also increase rapidly with the rise in slip parameter (see **Figure 3(c)**). Moreover, temperature profile and thermal boundary layer increase with an increase in solid nanoparticle volume fraction.

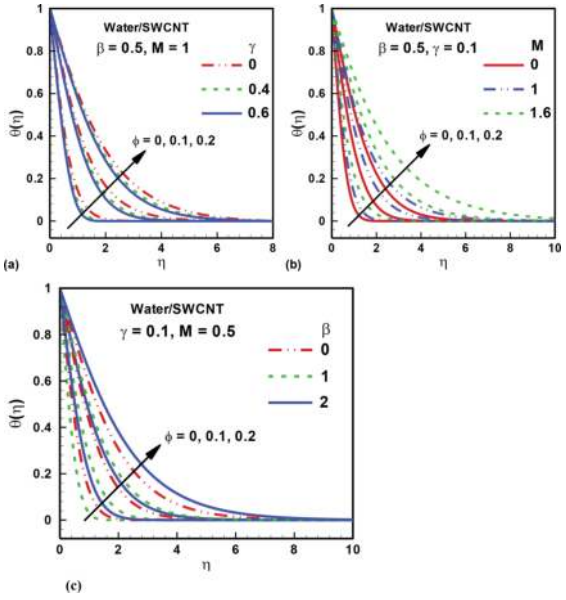

Figure 3. Temperature profile for different values of solid nanoparticle volume fraction. (a). Shows the variation with thermal relaxation time γ. (b) Shows the variation with Hartmann number M. (c) Shows the variation with slip parameter β.

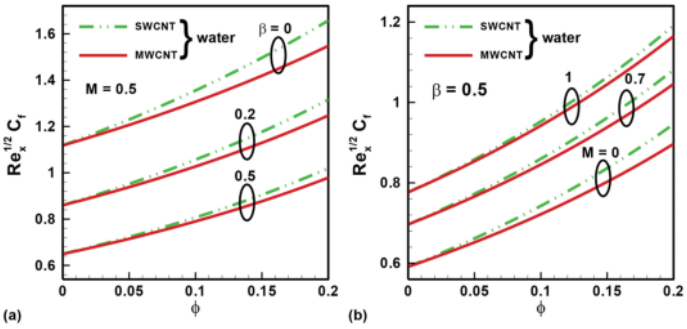

Figure 4. Skin friction coefficient for SWCNT and MWCNT. (a) Shows the variation with slip parameter β. (b) Shows the variation with Hartmann number M.

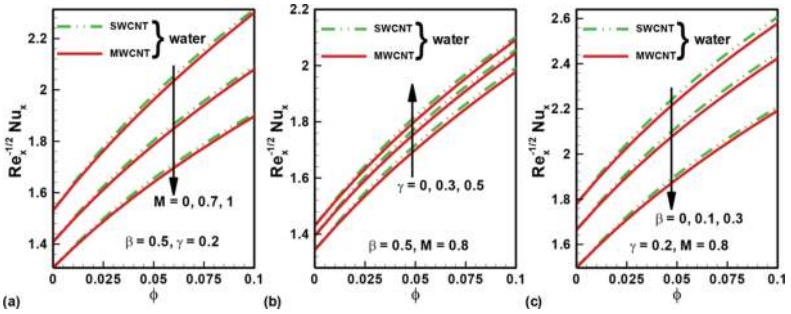

Figure 5. Nusselt number for SWCNT and MWCNT. (a) Shows the variation with Hartmann number M. (b) Shows the variation with thermal relaxation time γ. (c) Shows the variation with slip parameter β.

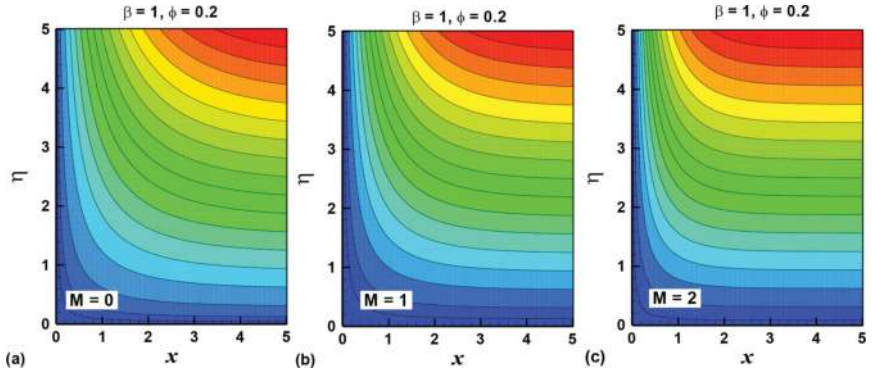

Figure 6(a-c). Streamlines for different values of Hartmann number M other parameters are β = 0.4, γ = 0.3.

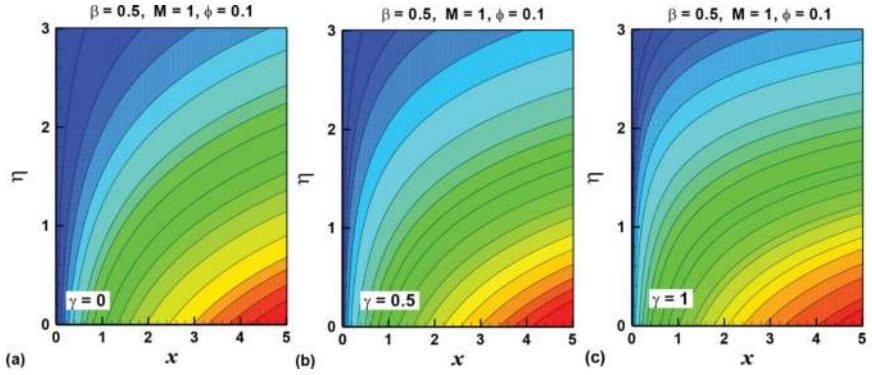

Figure 7(a-c). Isotherms for different values of thermal relaxation time γ other parameters are M = 2, β = 0.2.

Physical properties	Base fluid	Nanoparticles	
	Water	SWCNT	MWCNT
ρ (kg/m^3)	997	2600	1600
c_p (J/kg K)	4179	425	796
k (W/m K)	0.613	6600	3000

Table 1. Thermophysical properties of different base fluid and CNTs.

M	Present results	Salahuddin et al. [18]	Noreen et al. [19]
0.0	1	1	1
0.5	−1.11803	−1.11801	−1.11803
1	−1.41421	−1.41418	−1.41421
5	−2.44949	−2.44942	−2.44949
10	−3.31663	−3.31656	−3.31663
100	−10.04988	−10.04981	−10.04988
500	−22.38303	−22.38393	−22.38303
1000	−31.63859	−31.63846	−31.63859

Table 2. Comparison of results for the skin friction for pure fluid ($\phi = 0$).

Pr	Present results	Khan et al. [20]	Khan & Pop. [5]	Wang [11]	Kandasamy et al. [12]
0.07	0.0663	0.0663	0.0663	0.0656	0.0661
0.20	0.1691	0.1691	0.1691	0.1691	0.1691
0.70	0.4539	0.4539	0.4539	0.4539	0.4542
2	0.9114	0.9114	0.9113	0.9114	0.9114
7	1.8954	1.8954	1.8954	1.8954	1.8952
20	3.3539	3.3539	3.3539	3.3539	–
70	6.4622	6.4622	6.4621	6.4622	–

Table 3. Comparison of results for the Nusselt number for pure fluid ($\phi = 0$) with $M = 0$ and $\gamma = 0$.

ϕ		Cf			
		$M = 0$		$M = 0.5$	
		$\beta = 0$	$\beta = 1$	$\beta = 0$	$\beta = 1$
SWCNT	0.0	1	0.43016	1.11803	0.46912
	0.1	1.22904	0.54480	1.35495	0.58833
	0.2	1.51940	0.70245	1.65690	0.75286
MWCNT	0.0	1	0.43016	1.11803	0.46912
	0.1	1.17475	0.53298	1.30590	0.57942
	0.2	1.39935	0.67377	1.54755	0.73047

Table 4. Skin friction coefficient for different values of Hartmann number M and slip parameter β.

ϕ		Nusselt number							
		$\gamma = 0$		$\gamma = 0$		$\gamma = 0.1$		$\gamma = 0.1$	
		$M = 0$		$M = 0.5$		$M = 1$		$M = 2$	
		$\beta = 0$	$\beta = 1$	$\beta = 0$	$\beta = 1$	$\beta = 0$	$\beta = 1$	$\beta = 0$	$\beta = 1$
SWCNT	0.0	1.77095	1.33685	1.74513	1.25641	1.71287	1.08479	1.52688	0.70076
	0.1	2.66543	2.03231	2.60424	1.89346	2.48958	1.58280	2.07111	0.92785
	0.2	3.22397	2.49289	3.13585	2.31928	2.95535	1.92489	2.37985	1.11466
MWCNT	0.0	1.77095	1.33685	1.74513	1.25641	1.71287	1.08479	1.52688	0.70076
	0.1	2.63339	2.02350	2.57329	1.88386	2.46327	1.57551	2.05686	0.92736

Table 5. Nusselt number for different values of Hartmann number M and thermal relaxation time γ.

Variation in skin friction coefficient for SWCNT and MWCNT with slip parameter β and Hartmann number M is presented in **Figure 4**(**a** and **b**). It is seen that with the augment in M, electromagnetic strength is elevated in contrast to thick strength, skin friction coefficient rises for SWCNT as well as for MWCNT, but with the increase in slip parameter, skin friction coefficient decreases for both SWCNT and MWCNT. It is also seen that density and thermal conductivity of SWCNT are greater as compared to the MWCNT; therefore, the skin friction coefficient for SWCNT is greater as compared to the MWCNT.

Nusselt number for SWCNT and MWCNT shows the variation in Hartmann number M, thermal relaxation time γ, and slip parameter β. It is observed that the higher values of thermal relaxation time γ raise the Nusselt number for SWCNT as well as for MWCNT, and it is also analyzed that Nusselt number gives the larger values for SWCNT than MWCNT (see **Figure 5**(**a–c**)). Increasing values of Hartmann number M and slip parameter β decrease the Nusselt number for both SWCNT and MWCNT. But due to high density and thermal conductivity of SWCNT, Nusselt number for SWCNT is higher than MWCNT.

Streamlines and Isotherms are presented in **Figures 6**(**a–c**) and **7**(**a–c**), respectively. It is analyzed from **Figures 6** and **7** that for increasing Hartmann number M and thermal relaxation time γ, streamlines and Isotherms are going close to origin.

5. Conclusions

This chapter discussed the magnetic field effects on the flow of Cattanneo-Christov heat flux model for water-based CNT suspended nanofluid over a stretching sheet. Key points of the performed analysis are as follows:

1. It is observed that when Hartmann number increases, electromagnetic forces will be dominant to the viscous forces that give declines in the velocity.
2. It is analyzed that with an increase in slip parameter, velocity profile decreases. Further, with an increase in solid nanoparticle volume fraction, velocity profile increases.
3. Boundary layer thickness also increases with the increase in Hartmann number M, slip parameter β, and solid nanoparticle volume fraction φ.

http://dx.doi.org/10.5772/65628

4. Temperature profile decreases with the rise in thermal relaxation time, but thermal boundary layer increases with an increase in thermal relaxation time.

5. It depicts that with an increase in electromagnetic forces as compared to the viscous forces, temperature profile and thermal boundary layer increase rapidly.

6. Temperature profile and thermal boundary layer also increase rapidly with the rise in slip parameter.

7. Temperature profile and thermal boundary layer increase with an increase in solid nanoparticle volume fraction.

8. Skin friction coefficient increases for SWCNT as well for MWCNT, but with the increase in slip parameter, skin friction coefficient decreases for both SWCNT and MWCNT.

9. It is also seen that thickness and thermal conductivity of SWCNT are better as compared to the MWCNT; consequently, the skin friction coefficient for SWCNT is better as compared to MWCNT.

10. It is pragmatic that the superior values of thermal relaxation time γ hoist the Nusselt number for SWCNT as well as for MWCNT, and it is also analyzed that Nusselt number gives the well-built principles for SWCNT as evaluated to MWCNT.

11. It is analyzed from **Figures 6** and **7** that for rising Hartmann number M and thermal relaxation time γ, streamlines and isotherms are departing shut to source.

Nomenclature

μ_f: Viscosity of base fluid

$(\rho C_p)_f$: Effective heat capacity of a fluid

$(\rho C_p)_{CNT}$: Effective heat capacity of a carbon nanotubes

k_f: Thermal conductivities of the base fluid

k_{CNT}: Thermal conductivities of the carbon nanotubes

B_0: Magnitude of magnetic field strength

T: Local fluid temperature

T_∞: Ambient temperature

u, v: Velocity components along x and y directions

P: Pressure

ϕ: Nanoparticle volume fraction

q: Heat flux

U_w, V_w along the x-axis and y-axis: Thermal Grashof number

g: Acceleration due to gravity

λ_2: Thermal relaxation time

B_C: Solutal Grashof number

v: Kinematic viscosity of the fluid

P_r: Prandtl number

M: Hartmann number

$(\rho c_p)_{nf}$: Heat capacitance

ρ_{nf}: Effective density

Re_x: Local Reynolds number

η: Similarity variable (transformed coordinate)

α_{nf}: Effective thermal diffusibility

Nu_x: Local Nusselt number

x, y: Coordinate along and normal to the sheet

$(\rho c)_p$: Effective heat capacity of the nanoparticle material

$(\rho c)_f$: Heat capacity of the fluid

θ: Dimensionless temperature

μ_{nf}: Effective dynamic viscosity

γ: Non-dimensional thermal relaxation time

k_{nf}: Effective thermal conductivity of the nanofluid

Author details

Noreen Sher Akbar[1*], C. M. Khalique[2] and Zafar Hayat Khan[3]

*Address all correspondence to: noreensher1@gmail.com

1 DBS&H CEME, National University of Sciences and Technology, Islamabad, Pakistan

2 International Institute for Symmetry Analysis and Mathematical Modelling, Department of Mathematical Sciences, South Africa

3 Department of Mathematics, University of Malakand, Dir (Lower), Khyber Pakhtunkhwa, Pakistan

References

[1] S.U.S. Choi, Enhancing thermal conductivity of fluids with nanoparticles, in: D.A. Siginer, H.P. Wang (Eds.), Developments and Applications of Non-Newtonian Flows, ASME, New York, vol. 66 (1995) 99–105.

[2] Y. Xuan, W. Roetzel, Conceptions for heat transfer correlation of nanofluids, Int. J. Heat Mass Transfer. 43 (2000) 3701–3707.

[3] K. Khanafer, K. Vafai, M. Lightstone, Buoyancy-driven heat transfer enhancement in a two-dimensional enclosure utilizing nanofluids, Int. J. Heat Mass Transfer. 46 (2003) 3639–3653.

[4] A.V. Kuznetsov, D.A. Nield, Natural convective boundary-layer flow of a nanofluid past a vertical plate, Int. J. Therm. Sci. 49 (2010) 243–247.

[5] W.A. Khan, I. Pop, Boundary-layer flow of a nanofluid past a stretching sheet, Int. J. Heat Mass Tranfer 53 (2010) 2477–2483.

[6] A. Ebaid, H.A. El-arabawy, Y. Nader, New exact solutions for boundary-layer flow of a nanofluid past a stretching sheet, Int. J. Differential Equ. 2013 (Article ID 865464) 8.

[7] A. Ebaid, E.H. Aly, Exact analytical solution of the peristaltic nanofluids flow in an asymmetric channel with flexible walls: Application to cancer treatment, Comput. Math. Methods Med. 2013 (Article ID 825376) 8.

[8] A. Ebaid and A.M. Wazwaz, On the generalized Exp-function method and its application to boundary layer flow at nano-scale, J. Comput. Theor. Nanosci. 11(1) (2014) 178–184.

[9] A. Ebaid, E.H. Aly, N.Y. Abdelazem, Analytical and numerical investigations for the flow and heat transfer of nanofluids over a stretching sheet with partial slip boundary condition, J. Appl. Math. Inf. Sci. 8(4) (2014) 1639-1645.

[10] A. Ebaid, H.K. Al-Jeaid, H. Al-Aly, Notes on the Perturbation Solutions of the Boundary Layer Flow of Nanofluids Past a Stretching Sheet, Appl. Math. Sci. 7(122) (2013) 6077–6085.

[11] C.Y. Wang, Free convection on a vertical stretching surface, ZAMM J. Appl. Math. Mech. 69(11) (1989) 418–420.

[12] R. Kandasamy, P. Loganathan, P. Puvi Arasu, Scaling group transformation for MHD boundary-layer flow of a nanofluid past a vertical stretching surface in the presence of suction/injection, Nuclear Eng. Design 241(6) (2011) 2053–2059.

[13] B.J. Fourier, Theorie Analytique De Lachaleur, Jacques Gabay, Paris, 1822.

[14] C. Cattaneo, Sulla conduzionedelcalore, AttiSemin. Mat. Fis. Univ. Modena Reggio Emilia 3 (1948) 83–101.

[15] C.I. Christov, On frame indifferent formulation of the Maxwell–Cattaneo model of finite-speed heat conduction, Mech. Res. Commun. 36 (2009) 481–486.

[16] V. Tibullo, V. Zampoli, A uniqueness result for the Cattaneo–Christov heat conduction model applied to incompressible fluids, Mech. Res. Commun. 38 (2011) 77.

[17] M. Mustafa, Cattaneo–Christov heat flux model for rotating flow and heat transfer of upper convected Maxwell fluid, AIP Adv. 5 (2015) 047109.

[18] T. Salahuddin, M.Y. Malik, A. Hussain, S. Bilal, M. Awais, MHD flow of Cattanneo–Christov heat flux model for Williamson fluid over a stretching sheet with variable thickness: Using numerical approach, J. Magnet. Magnet. Mater. 401 (2016) 991–997.

[19] N.S. Akbar, E. Abdelhalim, Z.H. Khan, Numerical analysis of magnetic field effects on Eyring-Powell fluid flow towards a stretching sheet, J. Magnet. Magnet. Mater. 382 (2015) 355–358.

[20] Z.H. Khan, W.A. Khan, R.J. Culham, Estimation of boundary-layer flow of a nanofluid past a stretching sheet: A revised model, J. Hydrodyn. (2015).

[21] N.S. Akbar, Z.H. Khan, S. Nadeem, W.A. Khan, Double-diffusive natural convective boundary-layer flow of a nanofluid over a stretching sheet with magnetic field, Int. J. Numer. Methods Heat Fluid Flow 26(1) (2016) 108–121.

[22] M. Sheikholeslami, D.D. Ganji, M. Gorji-Bandpy, S. Soleimani, Magnetic field effect on nanofluid flow and heat transfer using KKL model, J. Taiwan Inst. Chem. Eng. 45 (2014) 795–807.

[23] H. Togun, G. Ahmadi, T. Abdulrazzaq, A.J. Shkarah, S.N. Kazi, A. Badarudin, M.R. Safaei, Thermal performance of nanofluid in ducts with double forward-facing steps, J. Taiwan Inst. Chem. Eng. 47 (2015) 28–42.

[24] M. Sheikholeslami, R. Ellahi, H.R. Ashorynejad, G. Domairry, Effects of heat transfer in flow of nanofluids over a permeable stretching wall in a porous medium, J. Comput. Theor. Nanosci. 11(2) (2014) 486–496.

[25] M. Sheikholeslami, D.D. Ganji, M.Y. Javed, R. Ellahi, Effect of thermal radiation on magnetohydrodynamics nanofluid flow and heat transfer by means of two phase model, J. Magnet. Magnet. Mater. 374 (2015) 36–43.

[26] M. Sheikholeslami, M. Gorji-Bandpy, Free convection of ferrofluid in a cavity heated from below in the presence of an external magnetic field, Powder Technol. 256 (2014) 490–498.

[27] M. Sheikholeslami, M. Gorji-Bandpy, D.D. Ganji, Lattice Boltzmann method for MHD natural convection heat transfer using nanofluid, Powder Technol. 254 (2014) 82–93.

[28] M. Sheikholeslami, M. Gorji-Bandpy, D.D. Ganji, Numerical investigation of MHD effects on Al_2O_3-water nanofluid flow and heat transfer in a semi-annulus enclosure using LBM, Energy 60 (2013) 501–510.

[29] M. Sheikholeslami, R. Ellahi, M. Hassan, S. Soleimani, A study of natural convection heat transfer in a nanofluid filled enclosure with elliptic inner cylinder, Int. J. Numer. Methods Heat Fluid Flow 24 (2014) 1906–1927.

[30] M. Sheikholeslami, M. Gorji, M. Bandpy, R. Ellahi, M. Hassan, S. Soleimani, Effects of MHD on Cu-water nanofluid flow and heat transfer by means of CVFEM, J. Magnet. Magnet. Mater. 349 (2014) 188–200.

[31] M. Sheikholeslami, M. Bandpy, M.G.R. Ellahi, R. Zeeshan, A simulation of MHD CuO-water nanofluid flow and convective heat transfer considering Lorentz forces, J. Magnet. Magnet. Mater. 369 (2014) 69–80.

[32] R. Ellahi, M. Gulzar, M. Sheikholeslami, Effects of heat transfer on peristaltic motion of Oldroyd fluid in the presence of inclined magnetic field, J. Magnet. Magnet. Mater. 372 (2014) 97–106.